The Astrophysical Journal, 954:146 (9pp), 2023 September 10 https://doi.org/10.3847/1538-4357/acea86

Energy Dissipation in Magnetic Islands Formed during Magnetic Reconnection

Quanming Lu[1,2,3], Kai Huang[1,2,3], Yundan Guan[1,2,3], San Lu[1,2,3], and Rongsheng Wang[1,2,3]
[1] Deep Space Exploration Laboratory, School of Earth and Space Sciences, University of Science and Technology of China, Hefei 230026, People's Republic of China; qmlu@ustc.edu.cn, inhk@ustc.edu.cn
[2] CAS Center for Excellence in Comparative Planetology, CAS Key Lab of Geospace Environment, Hefei 230026, People's Republic of China
[3] Collaborative Innovation Center of Astronautical Science and Technology, Harbin, People's Republic of China
Received 2023 May 23; revised 2023 July 8; accepted 2023 July 10; published 2023 September 1

Abstract

Magnetic reconnection converts magnetic energy into particle kinetic energy, and satellite observations have shown that 20%–50% of magnetic energy is channeled into electron kinetic energy. How such a large amount of magnetic energy is dissipated into electron kinetic energy is in debate. In this paper, by performing a large-scale 2D particle-in-cell simulation of magnetic reconnection with a guide field, we find that there exist both ion and electron shear flows in magnetic islands formed during magnetic reconnection, which are unstable to the ion and electron Kelvin–Helmholtz (K-H) instabilities. With the development of the K-H instabilities, the magnetic field lines are twisted in these magnetic islands, and intensified electron-scale current sheets are consequently generated. We quantitatively analyze the energy dissipation during such a process in magnetic islands and find that electrons obtain kinetic energy from the magnetic field while ion kinetic energy is transferred into magnetic energy. At last, it results that about 42% of magnetic energy is dissipated into electron kinetic energy in the whole process of magnetic reconnection. Our results help us better understand why a large amount of magnetic energy can be dissipated into electron kinetic energy.

Unified Astronomy Thesaurus concepts: Solar magnetic reconnection (1504); Space plasmas (1544); Solar energetic particles (1491)

Supporting material: animation

1. Introduction

As a ubiquitous physical process in plasma, magnetic reconnection, accompanied by the rearrangement of magnetic field lines, is considered to be an important driver for various explosive phenomena ranging from space and astrophysical to laboratory contexts (e.g., Parker 1957; Sweet 1958; Masuda et al. 1994; Tsuneta 1996; Gosling et al. 2005; Yamada et al. 2010; Burch et al. 2016; Torbert et al. 2018; Lu et al. 2022; Wang et al. 2023). In magnetic reconnection, magnetic energy is quickly dissipated into plasma kinetic energy (e.g., Lu et al. 2010; Egedal et al. 2012; Lu et al. 2013; Eastwood et al. 2013; Birn & Hesse 2014; Wilder et al. 2018; Burch et al. 2016; Yi et al. 2019; Shu et al. 2021; Huang et al. 2022; Sang et al. 2022; Chang et al. 2023), and satellite observations have indicated that up to 20%–50% of released magnetic energy is converted to electron kinetic energy (Lin et al. 2003; Holman 2005). Particle simulations have indicated that most of the magnetic energy is dissipated into ion kinetic energy in magnetic reconnection with a single X line (Yamada et al. 2014; Shu et al. 2021). Therefore, it is still an ongoing puzzle on how electrons can obtain such a large amount of kinetic energy during magnetic reconnection.

The diffusion region and magnetic island are two well-known sites that energize electrons (e.g., Hoshino et al. 2001; Drake et al. 2006; Fu et al. 2006; Pritchett 2006; Huang et al. 2010; Fu et al. 2011; Dahlin et al. 2014; Li et al. 2015; Wang et al. 2016; Lu et al. 2018). In the diffusion region, the enhancement of electron kinetic energy is caused by the induced reconnection electric field around the X line and jet fronts (Fu et al. 2006; Pritchett 2006; Huang et al. 2010; Fu et al. 2011; Wu et al. 2013; Huang et al. 2015; Huang et al. 2021). Electrons can also gain kinetic energy at the ends of a contracting magnetic island due to Fermi and betatron mechanisms (Drake et al. 2006; Fu et al. 2006; Dahlin et al. 2014; Wang et al. 2016; Lu et al. 2018). In the Fermi mechanism, electrons are accelerated by the motional electric field induced by the large-scale flows when they undergo the curvature drift; in the betatron mechanism, the electron energization is caused by the gradient B drift. Recently, a magnetic island formed during magnetic reconnection was found to be unstable to the electron Kelvin–Helmholtz instability, and at last, led to a turbulent state and intermittent reconnection (Huang et al. 2017). In this paper, by performing a 2D particle-in-cell (PIC) simulation, we further quantitively analyze the contribution of such a process to the energy dissipation during magnetic reconnection and find that it can enhance the dissipation rate from magnetic energy to electron kinetic energy.

2. Simulation Model

The VPIC code is employed in this paper to perform the 2D simulation of magnetic reconnection in the $x-z$ plane (Bowers et al. 2008). A Harris sheet with the magnetic field $\boldsymbol{B}(z) = B_0 \tanh(z/\delta)\mathrm{e}_x + B_g \mathrm{e}_y$ and plasma density $n(z) = n_0 \operatorname{sech}^2(z/\delta) + n_b$ is used as the initial configuration. Here, $B_g = B_0$ is the guide field, $n_b = 0.1 n_0$ is the background plasma density, and $\delta = 0.75 d_i$ is the half-width of the current sheet (d_i is the ion inertial length based on the peak Harris density n_0). The temperature ratio of ion to electron is $T_{i0}/T_{e0} = 5$, the light speed is $c = 20 V_A$ (V_A is the Alfvén speed defined by

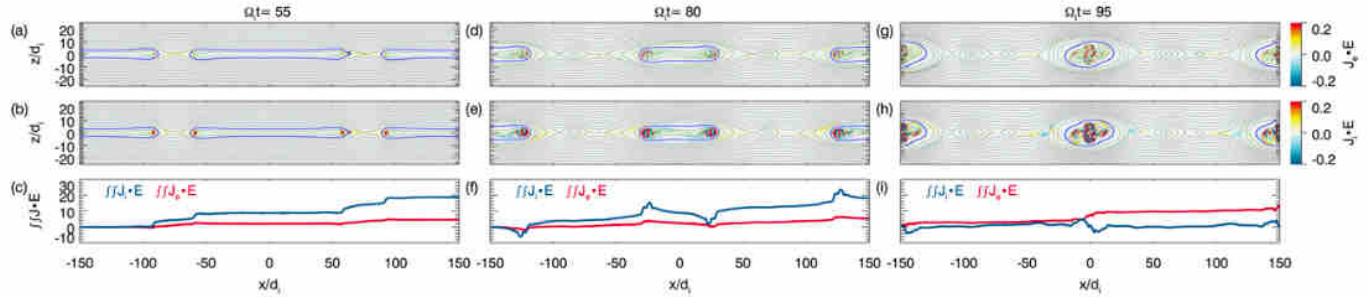

Figure 1. Spatial distribution of (a) electron energy dissipation $\boldsymbol{J_e} \cdot \boldsymbol{E}/(en_0V_A^2B_0)$, (b) the ion energy dissipation $\boldsymbol{J_i} \cdot \boldsymbol{E}/(en_0V_A^2B_0)$, and (c) their spatial integration $\int_{-L_x}^{x} dx', \int_{-L_z}^{L_z} \boldsymbol{J_e} \cdot \boldsymbol{E}dz'/(en_0V_A^2B_0d_i^2)$ and $\int_{-L_x}^{x} dx', \int_{-L_z}^{L_z} \boldsymbol{J_i} \cdot \boldsymbol{E}dz'/(en_0V_A^2B_0d_i^2)$ at $\Omega_it = 55$, 80, and 95. Reconnection occurs around $\Omega_it = 35$. The blue curves in (a) and (b) plot the field line with the magnetic flux function $\Psi = -22B_0d_i$ ($\Psi = 0$ at the z-directional boundaries).

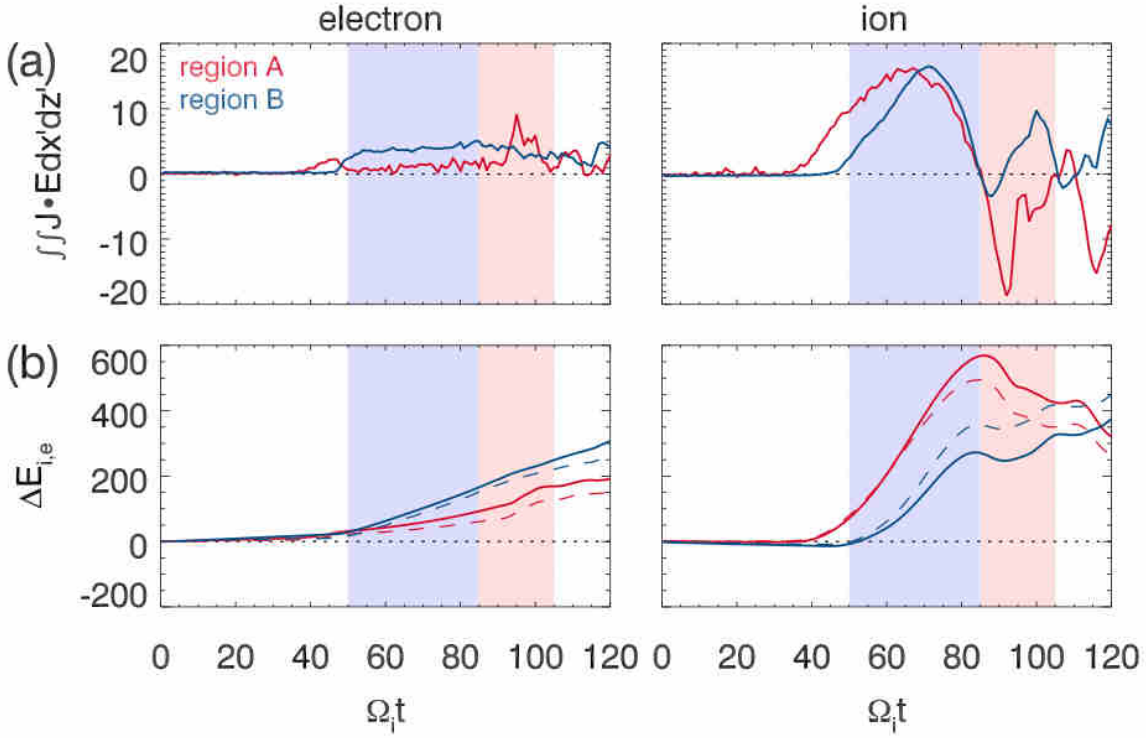

Figure 2. Time evolution of (a) electron energy dissipation $\iint \boldsymbol{J_e} \cdot \boldsymbol{E}dx', dz'/(en_0V_A^2B_0d_i^2)$ and ion energy dissipation $\iint \boldsymbol{J_i} \cdot \boldsymbol{E}dx'dz'/(en_0V_A^2B_0d_i^2)$, and (b) the increase in electron kinetic energy $\Delta E_e = E_e - E_{e0}$ and ion kinetic energy $\Delta E_i = E_i - E_{i0}$ (here E_{e0} and E_{i0} are electron and ion kinetic energy at $t = 0$, and all kinetic energy is normalized by $n_0m_iV_A^2d_i^2$) in Regions A and B. Here, Region A (red) is the region inside the circled blue lines in Figures 1(a) and (b), while Region B (blue) is the region outside the circled blue lines. In (b), kinetic energy denoted by the solid line is calculated by summing all particle kinetic energy, while that denoted by the dashed line is calculated by the time integration of the spatially integrated energy dissipation. The blue shadows denote the period when the magnetic islands are contracting, while the red shadows denote the period when the turbulence is active.

$V_A = B_0/\sqrt{\mu_0 m_i n_0}$), and the ion to electron mass ratio is set to be $m_i/m_e = 100$. The simulation domain is $[-L_x, L_x] \times [-L_z, L_z] = [-150d_i, 150d_i] \times [-25d_i, 25d_i]$ with a spatial resolution $\Delta x = \Delta z = 0.05d_i$. The time step is $\Delta t \approx 0.0017\Omega_i^{-1}$ ($\Omega_i = eB_0/m_i$ is the ion gyro-frequency). About 6×10^8 particles for each species are used in our simulation. Initial perturbations on the magnetic field at $x = \pm 75d_i$ are introduced to trigger magnetic reconnection. In the x direction, we use periodic boundary conditions; in the z direction, conducting boundary conditions are used for the electromagnetic field, and reflecting boundary conditions are used for particles.

3. Simulation Results

Magnetic reconnection begins to occur at about $\Omega_it = 35$, and two X lines appear around $x = -75d_i$ and $75d_i$. Please note that we use periodic boundary conditions in the x direction. Then, two magnetic islands are formed between the two X lines, which are around $x = -150d_i$ and 0. Figure 1 plots the distribution of (a) electron energy dissipation $\boldsymbol{J_e} \cdot \boldsymbol{E}$, (b) the ion energy dissipation $\boldsymbol{J_i} \cdot \boldsymbol{E}$, and (c) their spatial integration $\int_{-L_x}^{x} dx' \int_{-L_z}^{L_z} \boldsymbol{J_e} \cdot \boldsymbol{E}dz'$, and $\int_{-L_x}^{x} dx' \int_{-L_z}^{L_z} \boldsymbol{J_i} \cdot \boldsymbol{E}dz'$ at $\Omega_it = 55$, 80, and 95. At $\Omega_it = 55$, the energy dissipation occurs around the two X lines (around $x = -75d_i$ and $75d_i$) and the ends of

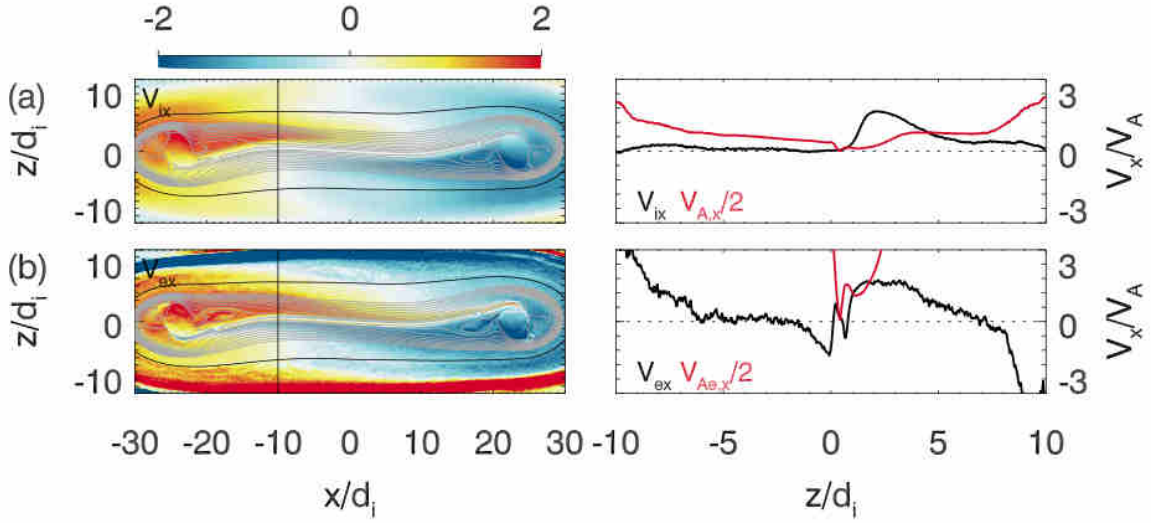

Figure 3. (a) The left panel shows the ion bulk velocity along the x-direction V_{ix}/V_A at $\Omega_i t = 80$, and the right panel plots the line profiles of V_{ix}/V_A and $V_{A,x}/(2V_A)$ at $x/d_i = -10$ (where $V_{A,x} = B_x/\sqrt{\mu_0 n_i m_i}$ is the local Alfvén speed). (b) The left panel shows the electron bulk velocity along the x-direction V_{ex}/V_A at $\Omega_i t = 80$, and the right panel plots the line profiles of V_{ex}/V_A and $V_{Ae,x}/(2V_A)$ at $x/d_i = -10$ (where $V_{Ae,x} = B_x/\sqrt{\mu_0 n_e m_i}$ is the local electron Alfvén speed).

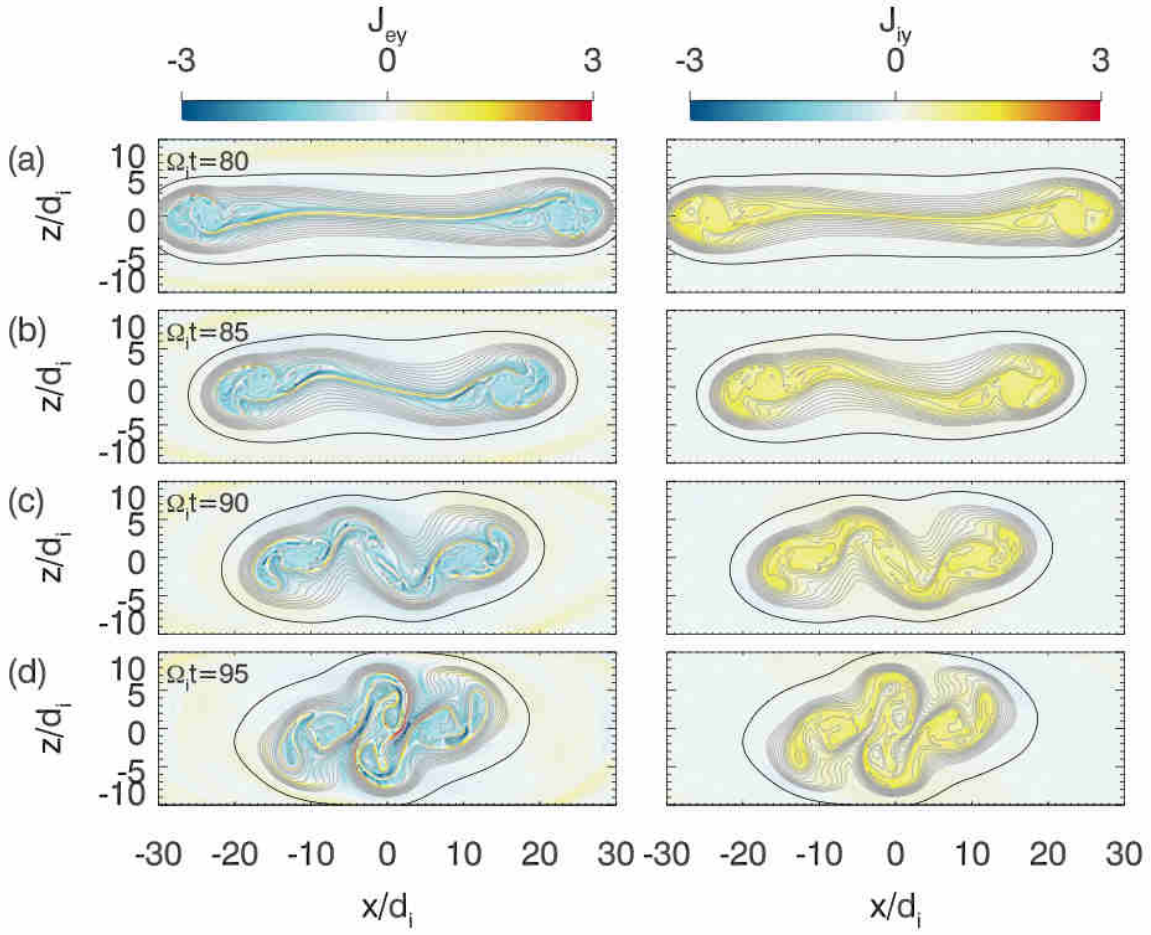

Figure 4. The electron current $j_{ey}/(en_0V_A)$ (left panel) and ion current $j_{iy}/(en_0V_A)$ (right panel) in the magnetic island around $x = 0$ at $\Omega_i t =$ (a) 80, (b) 85, (c) 90, and (d) 95.

two magnetic islands (around $x = -150d_i$ and 0), which has been thoroughly investigated in previous studies (Fu et al. 2006; Huang et al. 2010; Huang et al. 2015; Wang et al. 2016). At this time, we can also find that the ion energy dissipation is much larger than the electron energy dissipation. Because both of their values are positive, magnetic energy is dissipated into

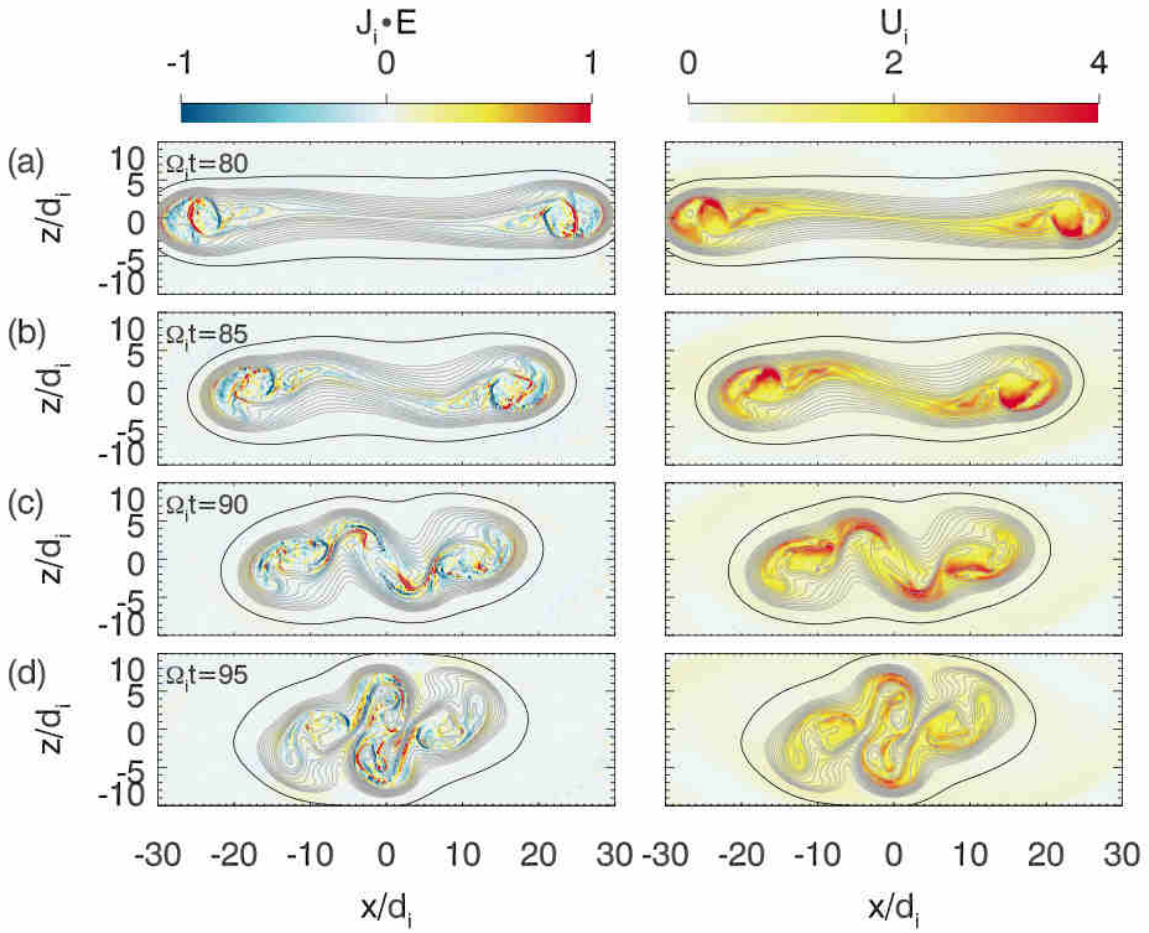

Figure 5. The ion energy dissipation $\boldsymbol{J_i} \cdot \boldsymbol{E}/(en_0V_A^2B_0)$ and the density of ion kinetic energy $U_i = n_i\bar{\varepsilon}_i/(n_0m_iV_A^2)$ (here, $\bar{\varepsilon}_i$ is the average of ion kinetic energy over each grid, and $\varepsilon_i = (\gamma - 1)m_ic^2$ is the ion kinetic energy, and they are normalized by $m_iV_A^2$) in the magnetic island around $x = 0$ at $\Omega_it =$ (a) 80, (b) 85, (c) 90, and (d) 95.

ion and electron kinetic energy. At $\Omega_it = 80$, two secondary islands begin to appear around $x = -85d_i$ and $70d_i$, which has been studied in detail (Daughton et al. 2006; Drake et al. 2006; Wang et al. 2010), but their contributions to energy dissipation are negligible. Both the ion and electron energy dissipations around the X line and two ends of each magnetic island are still positive. However, with the compression of the magnetic islands around $x = -150d_i$ and 0, both the ion and electron energy dissipations inside them become negative, and ion and electron kinetic energy are transferred to magnetic energy. At this time, the total ion and electron energy dissipation is still positive, and the total ion energy dissipation is much larger than the total electron energy dissipation. At $\Omega_it = 95$, the ion and electron energy dissipations around the two X lines are negligible. Ions can still obtain energy at the two ends of each magnetic island, but inside the magnetic islands ion kinetic energy is transferred into magnetic energy. However, inside the magnetic islands, the electron energy dissipation is still positive and electrons obtain energy from the magnetic field. The total energy dissipation of electrons becomes larger than that of ions. At the same time, we can also observe the twist of the magnetic field line inside the magnetic islands.

Figure 2 shows the time evolution of (a) electron energy dissipation $\iint \boldsymbol{J_e} \cdot \boldsymbol{E}dx', dz'$, and ion energy dissipation $\iint \boldsymbol{J_i} \cdot \boldsymbol{E}dx', dz'$, and (b) the increase in electron kinetic energy $\Delta E_e = E_e - E_{e0}$ and ion kinetic energy $\Delta E_i = E_i - E_{i0}$ (here E_{e0} and E_{i0} are electron and ion kinetic energy at $t = 0$) in Regions A and B. Here, Region A is the region inside the circled blue lines in Figures 1(a) and (b), while Region B is the region outside the circled blue lines. With the occurrence of magnetic reconnection at about $\Omega_it = 35$, both electron and ion kinetic energy begin to increase. For electrons, the energy dissipation is positive in both Region A and B, where electron kinetic energy increases continuously. At about $\Omega_it = 90$, the electron energy dissipation in Region A increases rapidly. For ions, the energy dissipation is almost always positive in Region B, where ion kinetic energy increases continuously. In Region

Table 1
Total Energy Increase $\Delta E/(n_0m_iV_A^2d_i^2)$ of Electrons and Ions in Regions A and B at $\Omega_it = 120$

	Increase in Electron Kinetic Energy	Increase in Ion Kinetic Energy
Region A	191.73	320.61
Region B	307.20	372.86
Total	498.93	694.47

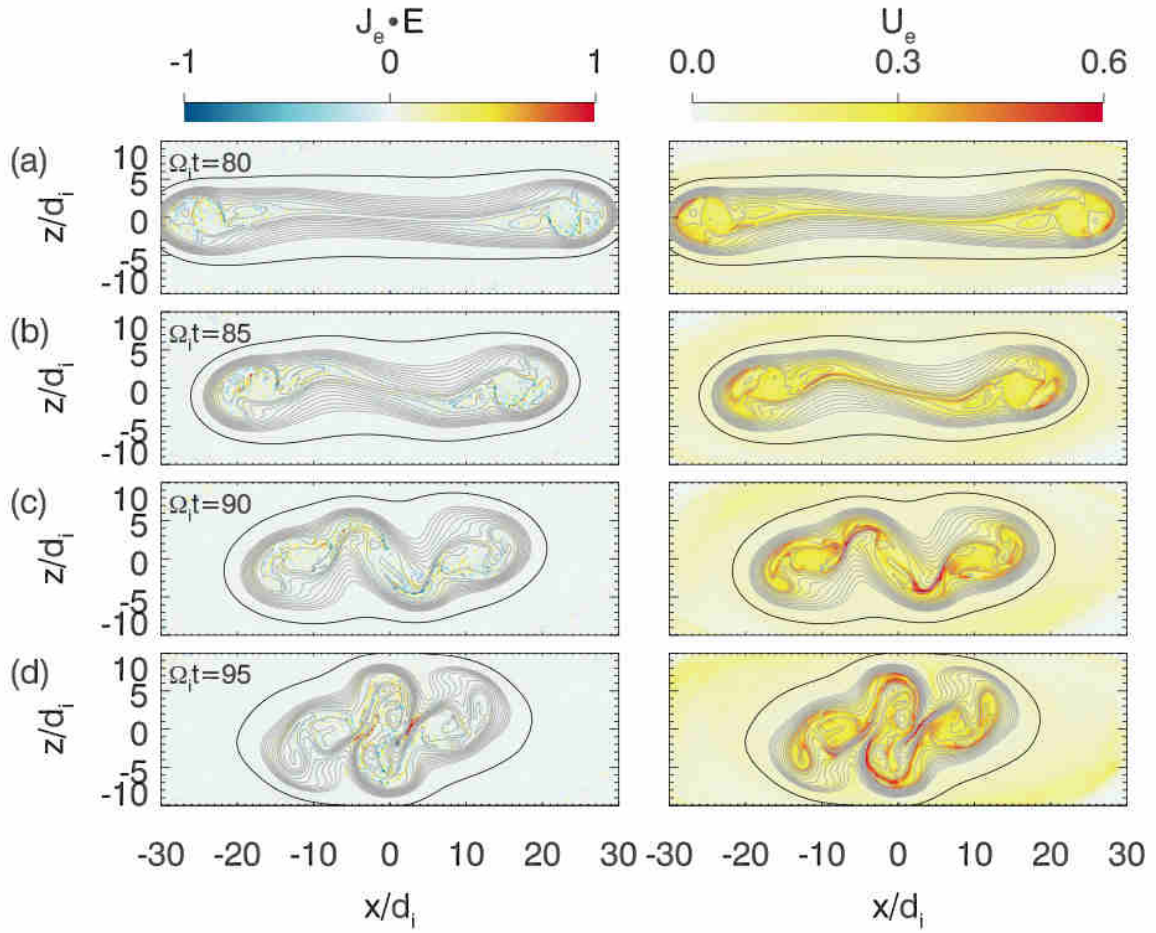

Figure 6. The electron energy dissipation $\boldsymbol{J_e} \cdot \boldsymbol{E}/(en_0V_A^2B_0)$ and the density of electron kinetic energy $U_e = n_e\bar{\varepsilon}_e/(n_0m_iV_A^2)$ (here, $\bar{\varepsilon}_e$ is the average of electron kinetic energy over each grid and $\varepsilon_e = (\gamma - 1)m_ec^2$ is the electron kinetic energy, and they are normalized by $m_iV_A^2$) in the magnetic island around $x = 0$ at $\Omega_it =$ (a) 80, (b) 85, (c) 90, and (d) 95.

A, the ion energy dissipation is first positive and then becomes negative from about $\Omega_it = 85$, which leads to the decrease of ion kinetic energy. In Table 1, we list the increase in ion and electron kinetic energy in both Regions A and B at $\Omega_it = 120$. At that time, the increases of electron and ion kinetic energy are 498.93 and $694.47n_0m_iV_A^2d_i^2$, and therefore about 42% of the release magnetic energy is transferred to electron kinetic energy. We have also calculated the increase in electron and ion kinetic energy in Regions A and B by the time integration of the energy dissipation, and they are almost the same as those by summing the kinetic energy of all ions and electrons. Obviously, the results obtained with the two ways are almost the same, which means that the energy transfer between Regions A and B is negligible. The increase or decrease of ion and electron kinetic energy in the magnetic islands is mainly determined by the energy dissipation.

The energy dissipation occurring in Region B is caused by the reconnection electric field. Here, we will focus on the physical mechanism of energy dissipation in Region A. Figures 3(a) and (b) exhibit the ion and electron bulk velocities along the x-direction at $\Omega_it = 80$, just before the strong magnetic fluctuations can be observed in the magnetic islands. In the left panel, we plot the distribution of ion bulk velocity V_{ix} and electron bulk velocity V_{ex} in the magnetic island around $x = 0$, which is circled by the blue line in Figure 1, while the right panel shows their values along the vertical lines denoted in the left panel. Obviously, strong ion and electron shear flows are formed in the magnetic island, and both ion and electron bulk velocities have positive values in the upper part and negative values in the lower part. Such kinds of ion and electron bulk velocities are related to the drift motion, which is caused by the Hall electric field E_z and the guide field, and such a process has been demonstrated in Huang et al. (2015). We can also find that the shear flows are unstable to both the ion and electron K-H instabilities: from the right panel, we can find that the variations of the bulk velocity satisfy the criterion of both the ion K-H instability $\Delta V_{ix} > V_{A,x}/2$ and electron K-H instability $\Delta V_{ex} > V_{Ae,x}/2$ (where $V_{A,x}$ and $V_{Ae,x}$ are the x-components of local ion and electron Alfvén speeds). Therefore, we conclude that the magnetic fluctuations inside the magnetic islands are caused by the ion and electron K-H instabilities.

With the excitation of both the ion and electron K-H instabilities in magnetic islands, the magnetic islands are distorted and current sheets are then formed. Figure 4 shows the electron current j_{ey} (left panel) and ion current j_{iy} (right panel) in the magnetic island around $x = 0$ at $\Omega_it =$ (a) 80, (b) 85, (c) 90, and (d) 95. During this time period, both the ion and

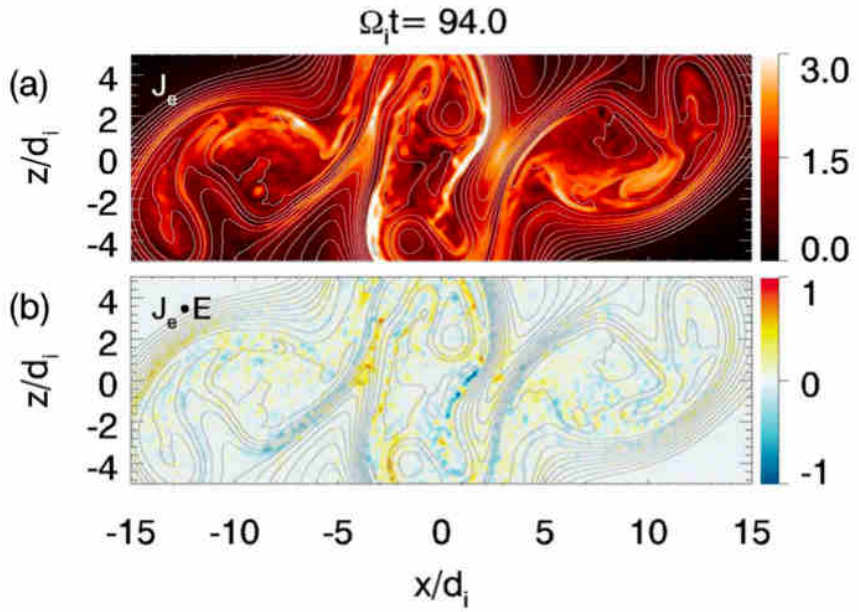

Figure 7. Time evolution of (a) the electron current $J_e/(en_0V_A)$ and (b) the energy dissipation $\boldsymbol{J_e}\cdot\boldsymbol{E}/(en_0V_A^2B_0)$ in the magnetic island around $x=0$ from $\Omega_i t=94$ to 99.1, and the time interval is $0.1\Omega_i^{-1}$. The gray curves represent the in-plane magnetic field lines. The continuous breaking and reconfiguration of these field lines accompanied by the large-amplitude J_e and $\boldsymbol{J_e}\cdot\boldsymbol{E}$ indicate the development of intermitted reconnection inside the magnetic island. More detailed information on one intermitted reconnection site at $\Omega_i t=95$ is shown in Figure 8. The real-time duration of the animation is 11 s.

(An animation of this figure is available.)

electron K-H instabilities are excited. Ion and electron current sheets are formed in the magnetic island with the twist of magnetic field lines, and the intensity of the electron current sheets is much stronger than that of ion current sheets. In situ evidence of the formation of current sheets in the K-H vortices has been provided by satellite observations in the Earth's magnetopause (Eriksson et al. 2016a; Li et al. 2016). The widths of ion current sheets are about several ion inertial lengths, while those of electron current sheets can be small to several electron inertial lengths.

In these current sheets, the energy transfer between the magnetic field and particles occurs. Figure 5 exhibits the ion energy dissipation $\boldsymbol{J_i}\cdot\boldsymbol{E}$, and the density of ion kinetic energy U_i in the magnetic island around $x=0$ at $\Omega_i t=(a)$ 80, (b) 85, (c) 90, and (d) 95. With the formation of current sheets in the magnetic island due to the excitation of the K-H instabilities, the ion energy dissipation becomes smaller than zero in most parts of the magnetic island, and ion kinetic energy becomes smaller and smaller in the magnetic island. This is consistent with that in Figure 2, where in the magnetic islands the ion kinetic energy is transferred into the magnetic energy. Figure 6 shows the electron energy dissipation $\boldsymbol{J_e}\cdot\boldsymbol{E}$, and the density of electron kinetic energy U_e in the magnetic island around $x=0$ at $\Omega_i t=(a)$ 80, (b) 85, (c) 90, and (d) 95. Here, the electron energy dissipation is positive in most parts of the magnetic island, and electron kinetic energy becomes larger and larger. Electrons obtain kinetic energy from magnetic energy in the magnetic island.

Intermittent magnetic reconnection can occur in these magnetic islands, which can be shown clearly in the animation associated with Figure 7. The time evolution of the electron current J_e and energy dissipation $\boldsymbol{J_e}\cdot\boldsymbol{E}$ in the magnetic island around $x=0$ from $\Omega_i t$=94 to 99.1 is shown clearly in the Figure 7 animation, and the magnetic field lines are also plotted. One intermittent magnetic reconnection event lasts usually about one to several ion cyclotron periods, and secondary islands may then be formed. In the vicinity of the X line, the electron currents are intensified, and there is strong electron energy dissipation. Magnetic reconnection in the magnetic island around $x=0$ can be shown more clearly in Figure 8, which plots (a) the parallel electric field $E_{\|}$, (b) the density of electron kinetic energy $U_e=n_e\bar{\varepsilon}_e$ (here, $\bar{\varepsilon}_e$ is the average of electron kinetic energy over each grid, and $\varepsilon_e=(\gamma-1)m_ec^2$ is electron kinetic energy), (c) the electron energy dissipation $\boldsymbol{J_e}\cdot\boldsymbol{E}$, and (d) the ion energy dissipation $\boldsymbol{J_i}\cdot\boldsymbol{E}$ at $\Omega_i t=95$. In the vicinity of the X line around $(x, z)=(2.5d_i, 0)$, there is strong electron energy dissipation and a parallel electric field, which leads to the enhancement of the electron energy flux. The ion energy dissipation may be positive or negative, and the net value is negative in the magnetic island, as described in Figure 1. Therefore, we can conclude that secondary magnetic reconnection in magnetic islands can dissipate magnetic energy into electron kinetic energy.

Figure 9 plots (a) the magnetic field, (b) the electron and ion density n, (c) the ion bulk velocity V_i/V_A, (d) the electron bulk velocity V_e/V_A, (e) the electric field E_M, (f) the temperature T, and (g) the electron energy dissipation $\boldsymbol{J_e}\cdot\boldsymbol{E}$. The X line moves along the L direction with a velocity of about $-0.4V_A$. The ion outflow and inflow velocities are about $0.8V_A$ and $0.2V_A$, and the electron outflow and inflow velocities are about $2V_A$ and $0.6V_A$. At the center of the current sheet, we can observe an obvious enhancement of the electron parallel temperature and electron energy dissipation, which is contributed by the parallel electric field and parallel electron current ($j_{e\|}E_{\|}$). The electron energy dissipation by the parallel electric field in guide magnetic

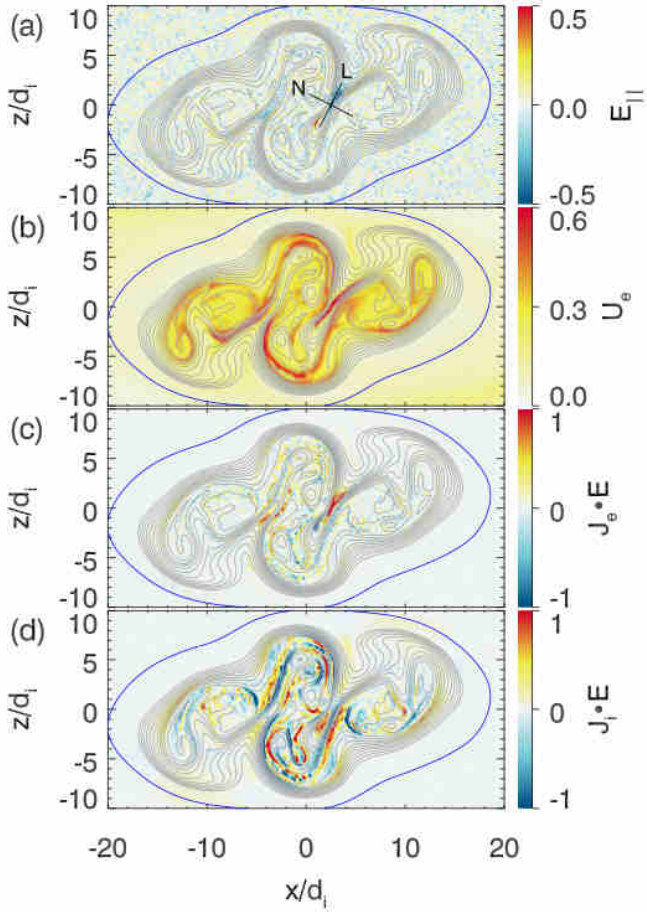

Figure 8. (a) the parallel electric field $E_{\parallel}/V_A B_{0\parallel}$, (b) the density of electron kinetic energy $U_e = n_e\bar{\varepsilon}_e/(n_0 m_i V_A^2)$, (c) the electron energy dissipation $\boldsymbol{J_e}\cdot\boldsymbol{E}/(en_0V_A^2B_0)$, and (d) the ion energy dissipation $\boldsymbol{J_i}\cdot\boldsymbol{E}/(en_0V_A^2B_0)$ at $\Omega_i t = 95$. The black cross in (a) shows the local L-N coordinate of the reconnecting current sheet.

reconnection has been thoroughly studied by both satellite observations (Eriksson et al. 2016b) and kinetic simulations (Pritchett 2006; Huang et al. 2010). The half-width of the current sheet can be estimated to be about $0.2d_i$ or $2d_e$, which is about 0.1 local ion inertial length or 1.0 local electron inertial length. The local Alfvén speed is about $0.6V_A$, and then according to the electric field in the M direction near the X line, we calculate the reconnection rate is about $1.0V_{A,l}B_l$ (where $V_{A,l}$ and B_l is the local Alfvén speed and reconnecting magnetic field). Obviously, this is an electron-scale reconnection event.

4. Conclusions and Discussion

In this paper, using a 2D PIC simulation model, we study a large-scale magnetic reconnection event with a guide field. Two X lines are formed by magnetic reconnection, where two magnetic islands are then generated. Both ion and electron shear flows exist in magnetic islands, which are unstable to the ion and electron K-H instabilities. Then, the magnetic field lines are twisted and intensified electron-scale current sheets are formed in the magnetic islands. Secondary magnetic reconnection occurs in these current sheets with the spatial scale down to a local electron inertial length. Besides the diffusion regions around the X lines and the ends of magnetic islands, the electrons can obtain kinetic energy from the magnetic energy due to secondary magnetic reconnection occurring in the magnetic islands. For the ions, they can only obtain kinetic energy from the magnetic field at the diffusion regions around the X lines and the ends of magnetic islands, while their kinetic energy is transferred into magnetic energy during the development of the K-H instabilities inside the magnetic island. Quantitative analysis has shown that such a process can largely enhance the dissipation rate from magnetic energy to electron kinetic energy. At last, about 42% of magnetic energy is dissipated into electron kinetic energy during magnetic reconnection.

Satellite observations of solar flares have indicated that 20%–50% of magnetic energy is transferred into electron kinetic energy during magnetic reconnection (Lin et al. 2003; Holman 2005). Our simulation has found that the K-H instabilities occur in magnetic islands within which secondary reconnection occurs. In situ observations have also revealed the twist of magnetic field lines and the formation of intensified current sheets in magnetic islands, where secondary magnetic reconnection occurs (Wang et al. 2020). Both our simulation and satellite observations have indicated that secondary magnetic reconnection in magnetic islands plays an important role in dissipating magnetic energy into electron kinetic energy. Our simulation further found that about 38% of the increase in the electron kinetic energy comes from secondary magnetic reconnection occurring in magnetic islands.

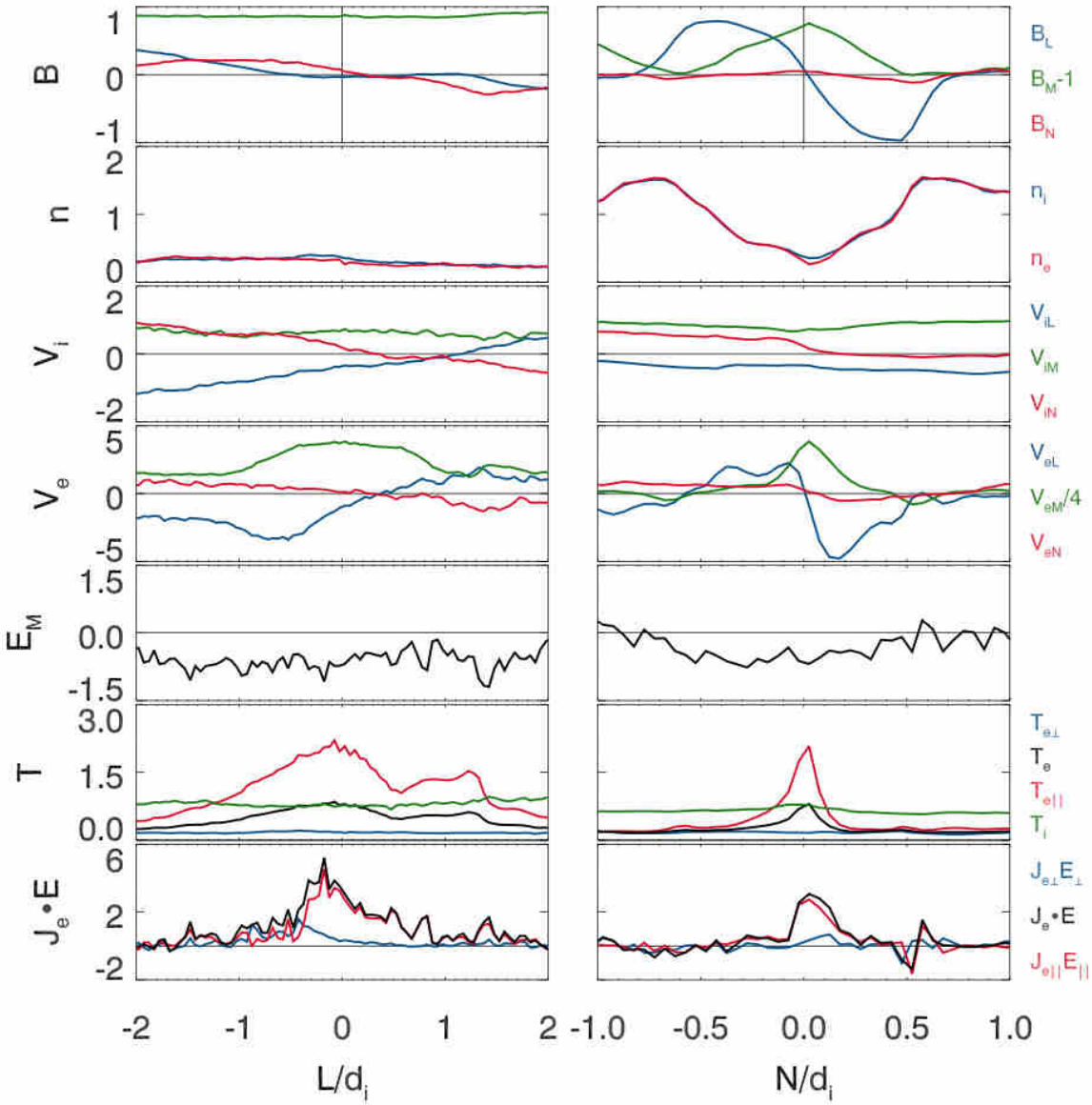

Figure 9. (a) the magnetic field B/B_0, (b) the electron and ion density n/n_0, (c) the ion bulk velocity V_i/V_A, (d) the electron bulk velocity V_e/V_A, (e) the electric field E_M/V_AB_0, (f) the temperature $T/m_iV_A^2$, and (g) the electron energy dissipation $\boldsymbol{J_e}\cdot\boldsymbol{E}/en_0V_A^2B_0$ along the L (left column) and N (right column) in Figure 5(a).

Acknowledgments

This work was supported by the National Key Research and Development Program of China (No. 2022YFA1604600), the NSFC grant 42174181, and the Strategic Priority Research Program of Chinese Academy of Sciences, grant No. XDB 41000000. The simulation was performed at the National Energy Research Scientific Computing Center (NERSC).

ORCID iDs

Quanming Lu https://orcid.org/0000-0003-3041-2682
Kai Huang https://orcid.org/0000-0003-3630-309X
San Lu https://orcid.org/0000-0003-2248-5072
Rongsheng Wang https://orcid.org/0000-0002-9511-7660

References

Birn, J., & Hesse, M. 2014, JGRA, 119, 290
Bowers, K. J., Albright, B. J., Yin, L., Bergen, B., & Kwan, T. J. T. 2008, PhPl, 15, 055703
Burch, J. L., Torbert, R. B., Phan, T. D., et al. 2016, Sci, 352, aaf2939
Chang, C., Huang, K., Lu, S., et al. 2023, ApJ, 943, 73
Dahlin, J. T., Drake, J. F., & Swisdak, M. 2014, PhPl, 21, 092304
Daughton, W., Scudder, J., & Karimabadi, H. 2006, PhPl, 13, 072101
Drake, J. F., Swisdak, M., Che, H., & Shay, M. A. 2006, Natur, 443, 553
Drake, J. F., Swisdak, M., Schoeffler, K. M., et al. 2006, GRL, 33, L13105
Eastwood, J P, Phan, T D, Øieroset, M, et al. 2013, PPCF, 55, 124001
Egedal, J., Daughton, W., & Le, A. 2012, NatPh, 8, 321
Eriksson, S., Lavraud, B., Wilder, F. D., et al. 2016a, GRL, 43, 5606
Eriksson, S., Wilder, F. D., Ergun, R. E., et al. 2016b, PhRvL, 117, 015001
Fu, H. S., Khotyaintsev, Y. V., André, M., & Vaivads, A. 2011, GeoRL, 38, L16104
Fu, X. R., Lu, Q. M., & Wang, S. 2006, PhPl, 13, 012309
Gosling, J. T. 2005, JGRA, 110, A01107
Holman, G. 2005, AdSpR, 35, 1669
Hoshino, M., Mukai, T., Terasawa, T., et al. 2001, JGRA, 106, 25979
Huang, C., Lu, Q. M., Wang, R. S., et al. 2017, ApJ, 835, 245
Huang, C., Lu, Q. M., & Wang, S. 2010, PhPl, 17, 072306
Huang, C., Wu, M., Lu, Q., Wang, R., & Wang, S. 2015, JGRA, 120, 1759
Huang, K., Lu, Q., Lu, S., Wang, R., & Wang, S. 2021, JGRA, 126, e2021JA029939
Huang, S. Y., Zhang, J., Yuan, Z. G., et al. 2022, GRL, 49, e2021GL096403
Li, W, Andre, M., Khotyaintsev, Yu. V., et al. 2016, GRL, 41, 5635

Li, X., Guo, F., Li, H., & Li, G. 2015, ApJL, 811, L24
Lin, R., Krucker, S., Hurford, G. J., et al. 2003, ApJL, 595, L69
Lu, Q. M., Fu, H. S., Wang, R. S., & Lu, S. 2022, ChPhB, 31, 089401
Lu, Q. M., Huang, C., Xie, J. L., et al. 2010, JGRA, 115, A11208
Lu, Q. M., Wang, H. Y., Huang, K., et al. 2018, PhPl, 25, 072126
Lu, S., Lu, Q., Huang, C., & Wang, S. 2013, PhPl, 20, 061203
Masuda, S., Kosugi, T., Hara, H., Tsuneta, S., & Ogawara, Y. 1994, Natur, 371, 495
Parker, E. N. 1957, JGR, 62, 509
Pritchett, P. L. 2006, JGRA, 111, A10212
Sang, L. L., Lu, Q. M., Xie, J. L., et al. 2022, PhPl, 29, 102108
Sweet, P. A. 1958, in Electromagnetic Phenomena in Cosmical Physics, ed. B. Lehnert (Cambridge: Cambridge Univ. Press)
Shu, Y. K., Lu, S., Lu, Q. M., Ding, W. X., & Wang, S. 2021, JGRA, 126, e29712
Torbert, R. B., Burch, J. L., Phan, T. D., et al. 2018, Sci, 362, 1391
Tsuneta, S. 1996, ApJ, 456, 840
Wang, H. Y., Lu, Q. M., Huang, C., & Wang, S. 2016, ApJ, 821, 84
Wang, R. S., Lu, Q. M., Du, A. M., et al. 2010, PhRvL, 104, 175003
Wang, R. S., Lu, Q. M., Nakamura, R., et al. 2016, NatPh, 12, 263
Wang, R. S., Wang, S. M., Lu, Q. M., et al. 2023, NatAs, 7, 18
Wang, S. M., Wang, R. S., Lu, Q. M., et al. 2020, NatCo, 11, 3964
Wilder, F. D., Ergun, R. E., Burch, J. L., et al. 2018, JGRA, 123, 6533
Wu, MingYu, Lu, QuanMing, Volwerk, Martin, et al. 2013, JGRA, 118, 4804
Yamada, M., Kulsrud, R., & Ji, H. 2010, RvMP, 82, 603
Yamada, M., et al. 2014, NatCo, 5, 4774
Yi, Y., Zhou, M., Song, L., & Deng, X. 2019, ApJL, 883, L22